11^{th} International Conference on Fracture Mechanics of Concrete and Concrete Structures
FraMCoS-11
J. M. Chandra Kishen, A. Ramaswamy, S. Ray and R. Vidyasagar (Eds)
https://doi.org/10.21012/FC11.092325

A PSO IDENTIFICATION PROCEDURE FOR PHASE FIELD FRACTURE MECHANICS PARAMETERS

Rakesh Kumar Tota *, **Marco Paggi**†

*IMT School for Advanced Studies Lucca, Piazza San Francesco
19, 55100, Lucca, Italy
e-mail: totarakesh.kumar@imtlucca.it

†IMT School for Advanced Studies Lucca, Piazza San Francesco
19, 55100, Lucca, Italy
e-mail: marco.paggi@imtlucca.it

Key words: Fracture mechanics, Phase field method, Particle swarm optimization, Parameters' identification, ABS co-polymers

Abstract. An algorithm implemented in MATLAB combining particle swarm optimization (PSO) and the phase field (PF) approach to fracture based on the finite element method is herein proposed to address the fundamental issue of model parameters' identification for phase-field fracture mechanics simulations. This work sheds further light on the role of the internal length scale parameter l_c, and the proposed robust PSO-PF formulation has been applied to a series of uni-axial tensile tests of ABS material with E and l_c to be identified, and to three-point bending tests with E, G_c and also l_c to be identified. Results show that the optimal values of E and G_c are consistent in both tests. At the same time, l_c presents a significant dependency upon the test type and, therefore, it should always be identified separately from uni-axial tests.

1 Introduction

The phase field approach to fracture is an emerging computational technique for the simulation of complex crack paths in solids and structures.

The development of numerical methods within the Finite Element Analysis (FEA) to predict fracture onset, propagation, and branching in materials and structures has been the subject of intensive research since the 1970s. Those methods are requested to tackle technical problems that analytical methods cannot address. In this regard, the Cornell Fracture Group [1] developed FEA software based on linear elastic fracture mechanics (LEFM). These methods were based on inserting singular finite elements at the crack tip to approximate the singular stress field and compute the stress-intensity factors according to the displacement correlation technique or the J-integral method. Although efficient for 2D problems, the extension of the methodology to 3D geometries, also with multiple materials, is quite complex since the theoretical definition of the generalized stress-intensity factors and the implementation of the related computational procedures require a significant effort [2].

Alternatively, Continuum Damage Mechanics (CDM) models accounting for a smeared crack representation [3] can address both crack nucleation and propagation stages. To avoid mesh dependency of local damage formulations, integral-based nonlocal and gradient-enhanced procedures have been proposed [4–8]. Moreover, extended FE strategies with

nodal kinematic enrichment (extended-FEM, X-FEM) that rely on Partition of Unity Methods (PUM) [9–11] and element enrichment formulations (enhanced-FEM, E-FEM) [12–15] have also seen a considerable development. These methods present limitations for the simulation of complex failure modes that require predicting crack initiation, propagation, branching, and coalescence from multiple points.

In this regard, the phase field (PF) approach to fracture proposed in [16] based on $\Gamma-$convergence [17] presents several advantages. The above approach incorporates a nonlocal formulation that can retrieve the classical energy-based Griffith criterion [18] as a limit case when the internal length scale of the model tends to zero. Significant progress has been made regarding the numerical implementation of the phase field approach to fracture in FEA codes, see e.g. [19–21]. This methodology appears to be very promising in reproducing not only the limit case of LEFM but also diffuse damage scenarios depending on the choice of the model parameters. It has been tested in relation to real experiments on brittle PMMA samples with notches and holes in [22]. Results have shown that the phase field approach to fracture can closely reproduce the experimental results not only in terms of the crack pattern but also in terms of force-displacement and local stress measures. In [22], parameters' identification for each type of simulated test was conducted manually. Still, preliminary results showed significant concerns, especially for the popular AT2 phase field model [19, 23] referred to as the standard Ambrosio-Tortorelli model in the applied mathematics community [24]. Specifically, the internal length scale of the phase field approach was quite a complex parameter to be identified.

The value of the peak traction in a simulated uni-axial tensile test is affected by the choice of the internal length scale of the phase field model. A possible correlation between material strength (σ_c) and the internal length scale (l_c) can be formally established, see [25], which has led to the wide belief that l_c estimated from uni-axial tensile tests can be consistently valid also for any other geometry and loading conditions. This belief has been questioned in [22], where manual identification of the internal length scale for all the conducted tests on PMMA samples with different geometry and loading conditions has shown that, especially for the AT2 model, it is not possible to use the value of the uni-axial tensile tests to reproduce all the experimental trends accurately. This motivates the need to develop a robust identification procedure to extract the optimal value of the internal length scale directly from experimental results. Thus, an automatic identification procedure is required and can be applied to evaluate the internal length scale parameter of the phase field model directly from the experimental data for conditions different from the uni-axial tensile tests.

Therefore, in this work, we outline a robust material parameters' identification procedure for the phase field approach to fracture based on Particle Swarm Optimization (PSO). The reader is referred to [26] for a detailed description of PSO applied to phase field fracture and additional sensitivity tests of the method, to demonstrate its robustness. The PSO heuristic approach has been demonstrated to be extremely robust in the case of mechanical problems involving multiple nonlinearities, as shown in [27], such as plasticity and cohesive fracture. Therefore it is considered an excellent candidate also for phase field diffuse damage. The article is structured as follows: in Section 2, the AT2 phase field approach is briefly outlined, highlighting the issue of parameters' identification. Section 3 focuses on the proposed model parameters' identification procedure in relation to a benchmark test related to PF fracture propagation. Section 4 discusses the application of the proposed methods to experimental data related to ABS specimens, showing how the algorithm can automatically identify the mean and the standard deviation of the phase field fracture parameters for uni-axial and three-point bending tests. ABS material has been selected for its importance in additive manufacturing and injec-

tion molding applications.

2 The phase field approach to fracture

Let us consider a linear elastic continuum domain $\Omega \subset \mathbb{R}^B$ in the reference configuration with dimension $B \in [1,3]$. A crack may nucleate and propagate from already-existing notches or stress-concentrated areas. The total potential energy functional of the continuum Ω proposed by Francfort-Marigo [16] with a prospective evolving crack surface Γ is given by

$$\begin{aligned}\Pi(\mathbf{u},\phi) = &\underbrace{\int_\Omega \Psi_E\left(\boldsymbol{\varepsilon}(\boldsymbol{u}),\phi\right)\mathrm{d}\Omega}_{\text{internal elastic energy}} \\ &+ \underbrace{\int_\Omega \Psi_S\left(\phi\right)\mathrm{d}\Omega}_{\text{energy due to crack propogation}} \\ &\underbrace{-\int_\Omega \mathbf{b}\mathbf{u}\,\mathrm{d}\Omega - \int_{\partial\Omega_t}\bar{\mathbf{t}}\mathbf{u}\,\mathrm{d}\partial\Omega}_{\text{external loads}}\end{aligned} \tag{1}$$

in which $\mathbf{b}$ and $\bar{\mathbf{t}}$ are body forces and boundary traction, respectively. $\Psi_E\left(\boldsymbol{\varepsilon},\phi\right)$ is the internal energy density function [20] defined as

$$\Psi_E\left(\boldsymbol{\varepsilon},\phi\right) = g(\phi)\Psi_0^+\left(\boldsymbol{\varepsilon}\right) + \Psi_0^-\left(\boldsymbol{\varepsilon}\right) \tag{2}$$

where $g(\phi) = (1-\phi)^2 + \kappa_p$ is the stress degradation function dependent upon the phase field damage variable ϕ, κ_p a small number to avoid ill-conditioning of the stiffness matrix for $\phi \to 1$. Ψ_0^+ and Ψ_0^- are the tensile and compressive energies respectively. Damaging the elastic energy of the material occurs only due to tensile stress states [28].

In the framework of the phase field regularization [29], $\Psi_S\left(\phi\right)$ the fracture energy contribution is smeared over the domain, and the surface integral (in 3D) or the line integral (in 2D) over Γ is approximated with an integral over the domain Ω:

$$\begin{aligned}\Psi_S(\phi) &:= \int_\Gamma G_c\,\mathrm{d}\Gamma \approx \int_\Omega G_c\gamma(\phi,\nabla\phi)\mathrm{d}\Omega \\ &\approx \frac{G_c}{2}\int_\Omega\left[l_c\nabla\phi\cdot\nabla\phi + \frac{\phi^2}{l_c}\right]\mathrm{d}\Omega\end{aligned} \tag{3}$$

where G_c is the fracture energy and l_c is the internal length scale parameter of the phase field.

The total energy functional therefore reads:

$$\begin{aligned}\Pi = &\int_\Omega\left(g(\phi)\Psi_0^+\left(\boldsymbol{\varepsilon}\right) + \Psi_0^-\left(\boldsymbol{\varepsilon}\right)\right)\mathrm{d}\Omega \\ &+ \int_\Omega \frac{G_c}{2}\left[l_c\nabla\phi\cdot\nabla\phi + \frac{1}{l_c}\phi^2\right]\mathrm{d}\Omega \\ &- \int_\Omega \mathbf{b}\mathbf{u}\,\mathrm{d}\Omega - \int_{\partial\Omega_t}\bar{\mathbf{t}}\mathbf{u}\,\mathrm{d}\partial\Omega_t\end{aligned} \tag{4}$$

The weak form of the problem is determined through the minimization of the above functional, which is done by computing its virtual variation with respect to the primary independent field variables:

$$\delta\Pi = \frac{\partial\Pi}{\partial\mathbf{u}}\delta\mathbf{u} + \frac{\partial\Pi}{\partial\phi}\delta\phi \tag{5}$$

which yields:

$$\begin{aligned}\delta\Pi = &\int_\Omega \sigma\delta\boldsymbol{\varepsilon}\,\mathrm{d}\Omega - \int_\Omega 2(1-\phi)\delta\phi\Psi_0^+\left(\boldsymbol{\varepsilon}\right)\mathrm{d}\Omega \\ &+ \int_\Omega G_c\left(l_c\nabla\phi\nabla\delta\phi + \frac{1}{l_c}\phi\delta\phi\right)\mathrm{d}\Omega \\ &- \int_\Omega b\delta u\,\mathrm{d}\Omega - \int_{\partial\Omega_t}\bar{t}\,\delta u\,\mathrm{d}\partial\Omega_t\end{aligned} \tag{6}$$

In addition to the above, to avoid healing of the material during damage evolution, an irreversibility condition upon ϕ has to be introduced. Again, we follow here the approach in [20], which introduces the following history variable $\mathcal{H}$ in Eq.(6).

$$\mathcal{H} = \begin{cases}\Psi_0^+(\boldsymbol{\varepsilon}) & \text{if } \Psi_0^+(\boldsymbol{\varepsilon}) > \mathcal{H}_n \\ \mathcal{H}_n & \text{otherwise}\end{cases} \tag{7}$$

where $\mathcal{H}_n$ is the value of Ψ_0^+ at the previous pseudo-time step of a quasi-static simulation with pseudo-time increasing applied displacements/loads. Note that the function $\mathcal{H}$ satisfies the Karush-Kuhn-Tucker conditions:

$$\Psi_0^+ - \mathcal{H} \leq 0, \dot{\mathcal{H}} \geq 0, \dot{\mathcal{H}}\left(\Psi_0^+ - \mathcal{H}\right) = 0 \tag{8}$$

The strong form associated to the weak from in Eq.(6) is:

$$\begin{aligned}&\nabla\cdot\sigma + \mathbf{b} = 0 \text{ in } \Omega, \quad \sigma\cdot n = \bar{t} \text{ on } \partial\Omega_{\bar{t}} \\ &u = \bar{u} \text{ on } \partial\Omega_u\end{aligned} \tag{9}$$

$$
\begin{aligned}
&- G_c l_c \nabla^2 \phi + \left[\frac{G_c}{l_c} + 2\Psi(\boldsymbol{\varepsilon}) \right] \phi = 2\Psi(\boldsymbol{\varepsilon}) \text{ in } \Omega \\
&\nabla \phi \cdot n = 0 \text{ on } \partial\Omega
\end{aligned}
\tag{10}
$$

To solve the above weak form, a four-nodes bilinear quadrilateral finite element discretization is introduced. Therefore in the FEM framework, at an elemental level, the displacement field $\mathbf{u}$ and the phase field ϕ are discretized by shape functions $\mathbf{N}_u$ and $\mathbf{N}_\phi$ expressed as follows. The corresponding derivatives of displacement and phase field values are also mentioned below:

$$
\begin{aligned}
\mathbf{u} &= \mathbf{N}_\mathbf{u} \mathbf{u}_e, \quad \phi = \mathbf{N}_\phi \phi_e \\
\boldsymbol{\varepsilon} &= \mathbf{B}_\mathbf{u} \mathbf{u}_e, \quad \nabla\phi = \mathbf{B}_\phi \phi_e
\end{aligned}
\tag{11}
$$

Similarly, the virtual variation terms of primary variables and their derivatives are defined as

$$
\begin{aligned}
\delta\mathbf{u} &= \mathbf{N}_\mathbf{u} \delta\mathbf{u}_e, \quad \delta\phi = \mathbf{N}_\phi \delta\phi_e \\
\delta\boldsymbol{\varepsilon} &= \mathbf{B}_\mathbf{u} \delta\mathbf{u}_e, \quad \nabla\delta\phi = \mathbf{B}_\phi \delta\phi_e
\end{aligned}
\tag{12}
$$

where $\mathbf{B}_\mathbf{u}$, $\mathbf{B}_\phi$ are the derivatives of the shape functions $\mathbf{N}_u$ and $\mathbf{N}_\phi$, respectively.

The arbitrariness of test functions leads to the following residual mechanical field and phase field vectors:

$$
\begin{aligned}
\mathbf{R}_\mathbf{u} = &\int_{\Omega^e} \mathbf{B}_\mathbf{u}^T \boldsymbol{\sigma} \, \mathrm{d}\Omega - \int_{\Omega^e} \mathbf{N}_\mathbf{u}^T \mathbf{b} \, \mathrm{d}\Omega \\
&- \int_{\partial\Omega^e} \mathbf{N}_\mathbf{u}^T \bar{\mathbf{t}} \, \mathrm{d}\partial\Omega
\end{aligned}
\tag{13}
$$

$$
\begin{aligned}
\mathbf{R}_\phi = &\int_{\Omega^e} G_c l_c \mathbf{B}_\phi^T \nabla\phi \, \mathrm{d}\Omega + \int_{\Omega^e} \frac{G_c}{l_c} \mathbf{N}_\phi^T \phi \, \mathrm{d}\Omega \\
&+ \int_{\Omega^e} 2\mathcal{H} \mathbf{N}_\phi^T \phi \, \mathrm{d}\Omega - \int_{\Omega^e} 2\mathbf{N}_\phi \mathcal{H} \, \mathrm{d}\Omega
\end{aligned}
\tag{14}
$$

The solution to the nonlinear problem can be achieved via the application of the Newton-Raphson solution scheme within a staggered approach, which requires the linearization of the residual vectors with respect to the field variables:

$$
\mathbf{K}_u = \frac{\partial \mathbf{R}_\mathbf{u}}{\partial \mathbf{u}} = \int_{\Omega^e} \mathbf{B}_\mathbf{u}^\mathrm{T} \mathbb{C} \mathbf{B}_\mathbf{u} \, \mathrm{d}\Omega \tag{15}
$$

$$
\begin{aligned}
\mathbf{K}_\phi = &\frac{\partial \mathbf{R}_\phi}{\partial \phi} = \int_{\Omega^e} G_c l_c \mathbf{B}_\phi^T \mathbf{B}_\phi \, \mathrm{d}\Omega \\
&+ \int_\Omega \left[\frac{G_c}{l_c} + \mathcal{H} \right] \mathbf{N}_\phi^T \mathbf{N}_\phi \, \mathrm{d}\Omega
\end{aligned}
\tag{16}
$$

The details of computation of the fourth order stiffness tensor $\mathbb{C}$ and the second order stress tensor $\boldsymbol{\sigma}$ are outlined in [28]. Therefore, the finite element implementation of the Phase field approach using the staggered solution scheme method [20] is implemented to find the displacement field and phase field solution.

3 Proposed parameters' identification procedure and benchmark tests

The issue of model parameters' identification for the phase field approach to fracture is relevant for technical applications, as outlined in the introduction. PSO has been proven to be a very effective tool in model parameters' identification for nonlinear fracture mechanics problems involving plasticity and cohesive fracture [27].

PSO [30] allows the scattering of certain populations of particles in a pre-defined parametric design space. PSO particles are then optimized by achieving a minimum target cost function (Υ) to match the user desired mechanical response. In the present problem, Young's modulus (E), fracture toughness (G_c), and the phase field internal length scale parameter (l_c) are the parameters defining each swarm particle position. Considering a force-displacement mechanical response (from experiments or desired), the target cost function (Υ) for every swarm particle is defined as

$$
\Upsilon(\chi) = \sqrt{\sum_{d=1}^{N} \left[\frac{\Delta F_d(\chi)}{\hat{F}_d(\chi)} \right]^2} \tag{17}
$$

where $\Delta F_d(\chi) = F_d - \hat{F}_d(\chi)$, in which F_d denotes the history of simulated forces for the range of imposed pseudo-time steps d ($d = 1, \ldots, N$). The simulated test is conducted under displacement control till 'N' number of imposed displacements for a given set of trial model parameters. Analogously, $\hat{F}_d(\chi)$ repre-

sents the target values of forces for the same 'N' imposed displacements.

As a benchmark test, to show the applicability of PSO to parameters identification of phase-field fracture models, we consider here a Mode I single edge notch test (see Fig.1). The following properties are set as an input for the simulation (E= 210 GPa, $G_c = 2.7$ kN/mm, $l_c = 0.1$ mm). The finite element discretization consists of 1949 four-noded bilinear quadrilateral finite elements with a minimum mesh size of 0.05 mm along the potential crack path. The force-displacement curve predicted by phase field simulation is taken as the target function $\hat{F}_d$. This should be subsequently matched by the PSO algorithm applied to identify the material parameters that are considered to be unknown.

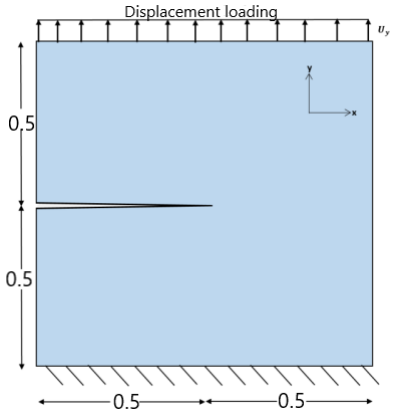

Figure 1: Benchmark problem: geometry, loading and boundary conditions.

In this regard, we attempt to identify all three material parameters simultaneously. In the 3D parameter space, we consider N_p = 30 particles as population size, a maximum of 150 iterations With the following PSO parameters: inertia weight $\mathbf{W_i} = 0.9$, damping weight $\mathrm{w_{damp}} = 0.99$. To assess the convergence of the PSO algorithm, the velocity of the constriction factor-based approach [31] is adopted here. The positive weights are applied to certain force-displacement points to set a priority while determining the cost function (Υ). If no positive weights are applied, all points in the force-displacement curve are treated equally. In the above-mentioned approach to guarantee stability [32], φ was set as 4.1 and $\mathbf{C_c} = \mathbf{S_c} = 2.05$. The design-constrained particle space is defined as follows:

$$\mathscr{Z} = \{180 < E < 230 \text{ GPa};\ 1.2 < G_c < 3.8 \text{ kN/mm};\ 0.02 < l_c < 0.2 \text{ mm}\} \tag{18}$$

which includes the values of the three parameters to be identified.

The evolution of swarm particles' position within the design space concerning PSO iterations are shown in Fig.4. The identified values of the model parameters were $E = 209.967$ GPa, $G_c = 2.699$ kN/mm, $l_c = 0.099$ mm, which are not too far from the parameters used to generate the target response numerically.

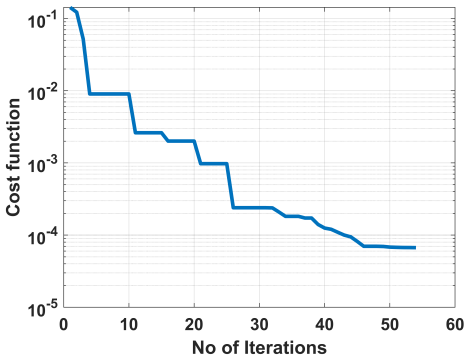

Figure 2: Cost function vs. No. of PSO iterations for the benchmark test.

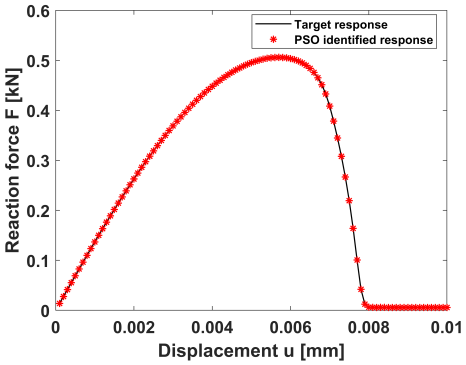

Figure 3: Force-displacement curve and target curve.

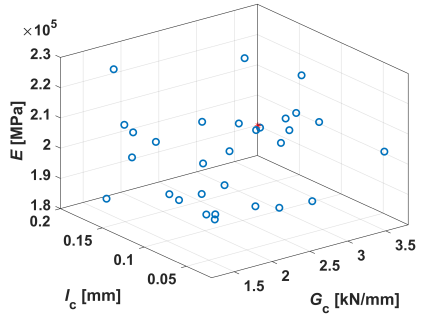

(a) Initial particles' position

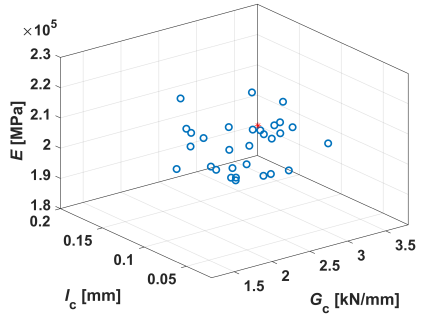

(b) Iteration No. 3

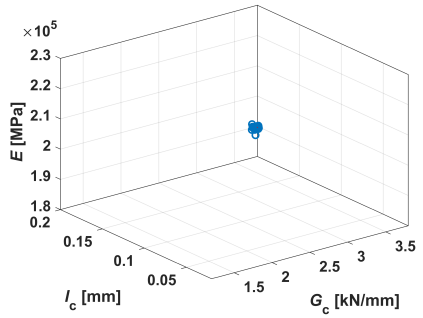

(c) Iteration No. 25

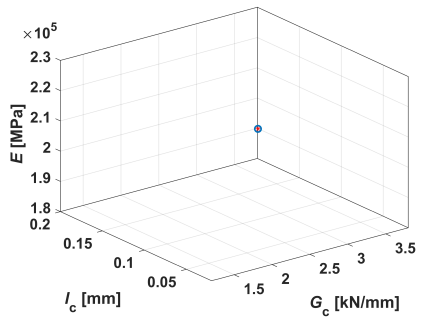

(d) Iteration No. 54

Figure 4: Scatter representation of particles in the iterations of the PSO algorithm for the benchmark test problem.

The cost function vs. a number of iterations is shown in Fig.2, with an error in the force-displacement curve at the 54th iteration lower than 1×10^{-4}.

For completeness, the force-displacement curve corresponding to the identified model parameters accurately matches the target one, see Fig.3.

Therefore, in the sequel, the PSO algorithm with the parameters considered above is applied to identify fracture mechanics parameters concerning the experimental results of ABS material discussed in Sec.4.

4 Identification of material properties from experimental data of ABS co-polymers

The robustness of the PSO algorithm applied to the identification of fracture mechanics parameters is herein assessed in relation to experimental results of ABS co-polymer material subjected to tensile and three-point bending loading conditions.

A series of uni-axial and three-point bending experimental tests were carried out. The scatter in the experimental curves shown in Figs.6(a) and 8(a) is due to the typical effect induced by a slight variation in the amount of additives used to reduce swelling in ABS materials for injection moulding [33].

The PF formulation based on the AT2 model has been applied to simulate the corresponding tests, and coupled with the PSO algorithm, parameter identification has been performed. All the routines are coded in MATLAB, release 2020b.

Young's modulus E, fracture parameters G_c (fracture energy), and l_c (internal length scale) were chosen as PSO swarm particle parameters to be identified. The range of ABS properties to conduct PSO-PF simulations were taken from literature: tensile strength $\sigma_{\max} \in \{22, 49\}$ MPa, $E \in \{1100, 2900\}$ MPa, Poisson's ratio ν = 0.37 and fracture toughness $K_{I,c} \in \{1.2, 4.2\}$ MPa$\sqrt{m}$. Exploiting the correlations $G_c = \frac{\mathrm{K}_{I,c}^2(1-\nu^2)}{E}$ and $l_c = \frac{27}{256}\frac{G_c E}{(1-\nu^2)\sigma_{\max}^2}$, we derived the following range of variability for $G_c \in \{1.25, 13.8\}$ N/mm and $l_c \in \{0.25, 3.8\}$

mm.

4.1 Uni-axial tensile tests

Experimental tests were conducted and repeated 15 times on specimens of ABS material under uni-axial tensile loading conditions. The specimen geometry is length $\times$ width $\times$ thickness = $114 \times 10.2 \times 4.5$ mm. The boundary conditions are depicted in Fig.5. Stress-strain curves are shown in Fig.6(a). PF numerical simulations have been performed by replicating the experimental conditions (see Fig.5). Dirichlet boundary condition $\phi = 0$ [34, 35] imposed on the phase field at both ends of the tensile test model.

Since uni-axial tensile tests are unsuitable for fracture mechanics characterization, we set an average value of $G_C = 7.5$ N/mm from the literature for all 15 numerical simulations. E and l_c are the parameters to be identified that influence the initial linear elastic regime of the stress-strain curves and the material tensile strength (computed from the peak load value before specimen failure). Therefore, the PF-PSO simulations are conducted with swarm particles in the parameter space (E, l_c), with admissible range for $E \in \{1100, 2900\}$ MPa and for $l_c \in \{0.25, 3.8\}$ mm. Fig.6(b) shows the optimal PSO-PF response of the 15 stress-strain curves that minimize the error from the experimental ones. Table 1 collects the PSO-identified parameters for the 15 tests. From this analysis, considering the mean values and the standard deviations, the identified Young modulus corresponds to $\overline{E} \pm \sigma_E = 1157.904.01 \pm 34.8223$ MPa, and the internal length scale $\overline{l}_c \pm \sigma_{l_c} = 1.3361 \pm 0.0408$ mm.

4.2 Three-point bending tests

Three-point bending tests with notched samples are now considered since they can also be exploited for fracture mechanics characterization. Therefore, applying the PSO algorithm combined with the PF simulation framework is possible to identify all three model parameters, E, l_c, and G_c. Now these are critically compared with the outcome of the previous parameters' identification results concerning uni-axial tensile tests.

Experimental tests were conducted on a set of ABS specimens with an initial sharp V-notch under the three-point bending loading, see Fig.7(a) and (b), showing the initially undeformed configuration and the specimen at failure. Fig.7(b) shows the formation of crazing at the notch tip, which is highlighted by the change of color of ABS from yellow to white due to the stretching of the polymeric fibers during crack growth. The spread of crazing in the direction orthogonal to the mid-span cross-section is relatively consistent. It certainly represents a zone of diffuse damage that could be simulated using the phase-field approach to fracture with a finite -not vanishing- internal length scale l_c. Compared to PMMA investigated in [22], ABS is much less brittle.

The geometrical data are shown in Fig.7(c). Fig.7(d) depicts an FE mesh with linear quadrilateral finite elements with a fine discretization near the mid-cross-section and a coarser one far from the perspective crack path. A preliminary mesh sensitivity analysis has been performed for the PF simulations, considering 1614, 7076, or 13984 finite elements using different degrees of refinement of the mesh far from the mid-cross-section. The numerical predictions were almost unaffected if the mid-cross-section was properly discretized. The discretization in 1614 FE has been considered for the parameter identification issue to speed up computation time.

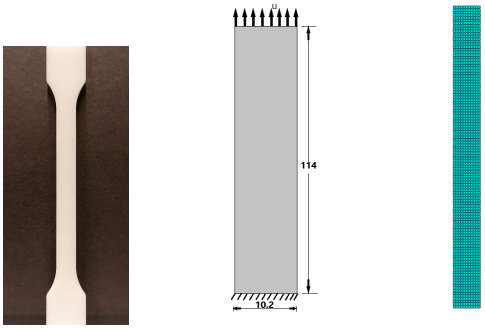

Figure 5: (a) Photo of the specimen, (b) Dimensions and boundary conditions, (c) FE mesh.

Table 1: PSO identified E and l_c parameters for the 15 tests in Fig.6, with their mean and standard deviation values.

Test #	E (MPa)	l_c (mm)
1	1130.39	1.281
2	1116.48	1.306
3	1215.08	1.415
4	1197.61	1.362
5	1183.24	1.320
6	1169.18	1.359
7	1120.50	1.290
8	1164.82	1.321
9	1123.67	1.273
10	1141.05	1.330
11	1107.73	1.392
12	1193.60	1.376
13	1152.43	1.318
14	1203.60	1.347
15	1149.19	1.351

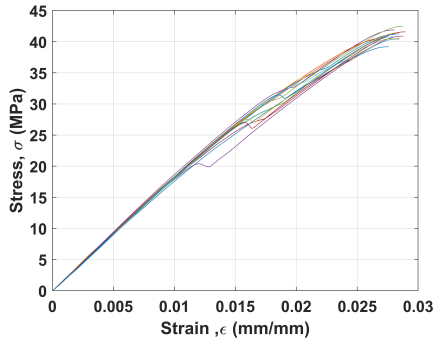

(a) Experimental results

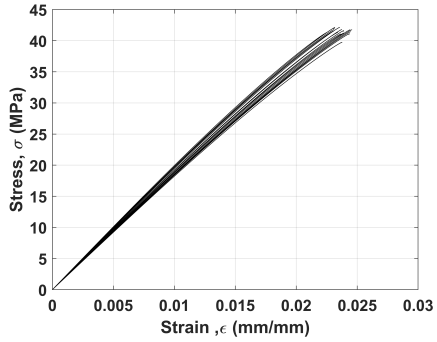

(b) Numerical simulations

Figure 6: Experimental and numerical simulation results identified (corresponding to the identified model parameters).

Force vs. mid-span displacement curves for the 15 tests are shown in Fig.8. It compares the experimental curves (left panel) with the results of the numerical simulations (right panel) corresponding to the identified best model parameters by the PSO algorithm. Again, the following range of values has been considered $E \in \{1100, 2900\}$ MPa, $G_c \in \{1.25, 13.8\}$ N/mm, $l_c \in \{0.25, 3.8\}$ mm.

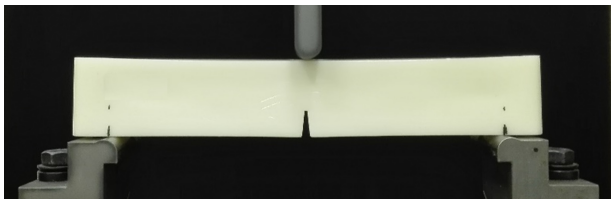

(a) Undeformed specimen

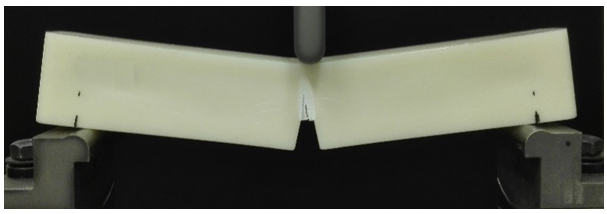

(b) Deformed specimen at failure

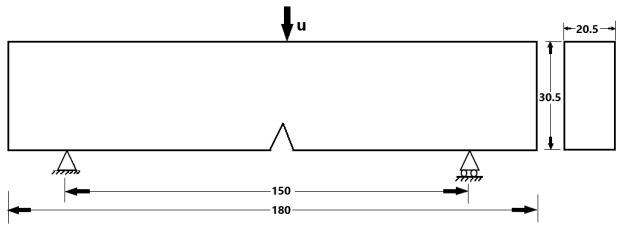

(c) Geometry and boundary conditions (measures in mm)

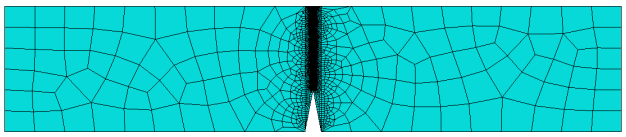

(d) FE model

Figure 7: Experiment specimen and geometrical details (in mm), loading, boundary condition, meshing details of a numerical model for three-point bending loading case

Table 2 collects all the identified parameters E, G_c, and l_c, with their respective mean values and standard deviations. Results can now be compared with the outcome of the identification performed on uni-axial tensile tests of

the same materials, and that was limited to two model parameters, E and l_c. The identified Young modulus in the case of three-point bending tests was 1153.07 ± 35.03 MPa, and it is very close to the identified Young's modulus from the uni-axial tensile tests, which was estimated as 1157.90 ± 34.82 MPa. The identified fracture toughness from three-point bending tests is 8.85 ± 1.94 N/mm, and it compares well with the average value taken from the literature and is equal to 7.5 N/mm that was set for all the uni-axial tensile tests. On the other hand, a significant discrepancy is observed as far as the internal length scale parameter l_c is concerned. The identified value from the three-point bending tests is 0.346 ± 0.157 mm, while from the uni-axial tensile tests, it was 1.336 ± 0.041 mm. In addition to being smaller, the scatter also increased, as one can notice from the higher standard deviation value. Henceforth inverse analysis procedure is strongly recommended to identify length scale parameters for different geometry loading test problems [36].

Table 2: PSO identified E, G_c and l_c parameters for the 15 tests in Fig.8, with their mean and standard deviation values.

Test #	E (MPa)	G_c (N/mm)	l_c (mm)
1	1189.39	7.56	0.250
2	1189.67	7.56	0.250
3	1101.17	8.83	0.256
4	1173.92	7.18	0.251
5	1176.29	7.84	0.250
6	1158.87	8.29	0.252
7	1179.82	7.38	0.290
8	1178.73	7.37	0.291
9	1133.36	8.35	0.303
10	1100.58	12.28	0.649
11	1100.40	12.21	0.639
12	1167.95	7.63	0.250
13	1139.86	10.23	0.369
14	1113.41	12.40	0.642
15	1192.62	7.62	0.256
Mean	1153.07	8.85	0.346
Std. dev. (STD)	35.03	1.94	0.157

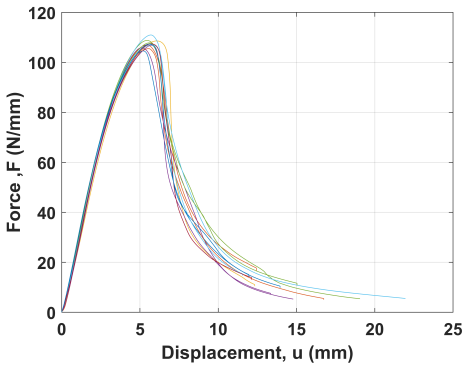

(a) Experimental results

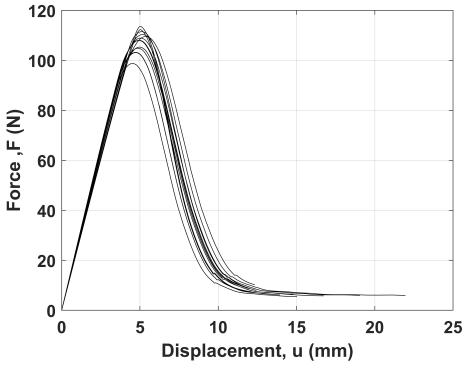

(b) Numerical simulation results

Figure 8: Representation of experimental and numerical simulations of 15 force-displacement curve results.

5 Conclusion

The critical issue of model parameters' identification for the phase field approach to fracture has been systematically addressed in this work. The proposed framework combines the heuristic identification approach based on Particle Swarm Optimization (PSO) and the FE implementation of the phase field (PF) approach to fracture, which has effectively identified model parameters. Both formulations have been implemented in MATLAB release 2020b in an ad hoc integrated FE software. Still, the methodology is general and requires a FE solver equipped with PF finite elements to be called by the PSO algorithm with a set of model parameters. The outcome of the FE simulation, in terms of the force-displacement curve, is again passed to the PSO algorithm, which computes the cost function and updates the particle coor-

dinates, iterating the procedure till convergence. Therefore, any commercial FE software could be triggered using the system command called by the PSO algorithm.

The robustness of the proposed approach has been assessed in relation to a benchmark test numerically generated in silico, i.e., by running a PF fracture simulation with known model parameters. The PSO algorithm could accurately retrieve the known input parameters from the identification procedure.

The methodology has been finally applied to the critical problem of identifying the AT2 PF model parameters concerning real experimental tests on ABS materials which display a spread of diffuse damage typical of a quasi-brittle material. First, the PSO-PF combined approach has been applied to uni-axial tensile tests, identifying only E and l_c from the experimental curve up to the decay of the peak load. The uni-axial tests for this material cannot be used to assess the fracture energy, which has been set equal to the average value taken from the literature since the material undergoes strain localization with the crazing formation and large deformation in the post-peak branch, a situation far from the fracture. The identification procedure has been repeated for sharp V-notched samples tested under three-point bending. This time, all the three model parameters (E, G_c, l_c) are identified since the post-peak branch can be reasonably well simulated as a result of a propagating crack.

To summarize the work, the proposed algorithm quantitively tracks the crack path phenomenon of the fracture problem. In addition, it also captures numerically experimental force-displacement curve responses by identifying phase field model parameters, which is a significant challenge due to the high dependence on the PF internal length scale parameter. Therefore PSO-PF numerically coupled algorithm provides a qualitative insight into the fracture design problems in avoiding under or overestimating critical structural limits of the load, which saves computational time and the cost of the material.

REFERENCES

[1] P.A. Wawrzynek and A.R. Ingraffea. Interactive finite element analysis of fracture processes: an integrated approach. *Theoretical and Applied Fracture Mechanics*, 8:137–150, 1987.

[2] M. Paggi and A. Carpinteri. On the Stress Singularities at Multimaterial Interfaces and Related Analogies With Fluid Dynamics and Diffusion. *Applied Mechanics Reviews*, 61(2), 2008. 020801.

[3] J. Lemaitre and R. Desmorat. *Engineering Damage Mechanics: Ductile, Creep, Fatigue and Brittle Failures*. Springer-Verlag, Berlin, 2005.

[4] Z.P. Bažant and T.G.P. Pijaudier-Cabot. Nonlocal continuum damage, localization instability and convergence. *Journal of Applied Mechanics*, 55:287–293, 1988.

[5] M. Jirásek. Nonlocal models for damage and fracture: Comparison of approaches. *Int. J. Solids Struct.*, 35:4133–4145, 1998.

[6] S. Forest. Micromorphic approach for gradient elasticity, viscoplasticity, and damage. *Journal of Engineering Mechanics*, 135:117–131, 2009.

[7] B.J. Dimitrijevic and K. Hackl. A regularization framework for damage-plasticity models via gradient enhancement of the free energy. *Int. J. Numer. Methods Biomed. Eng.*, 27:1199–1210, 2011.

[8] R. Peerlings, M. Geers, R. de Borst, and Brekelmans W. A critical comparison of non local and gradient-enhanced softening continua. *Int. J. Solids Struct.*, 38:7723—-7746, 2001.

[9] N. Moës, J. Dolbow, and T. Belytschko. A finite element method for crack growth without remeshing. *Internat. J. Numer. Methods Engrg.*, 46:131–150, 1999.

[10] J. Dolbow, N. Moës, and T. Belytschko. An extended finite element method for

modeling crack growth with contact. *Comput. Methods Appl. Mech. Engrg.*, 190:6825–6846, 2001.

[11] T.P. Fries and T. Belytschko. The extended/generalized finite element method: an overview of the method and its applications. *Internat. J. Numer. Methods Engrg.*, 84:253–304, 2010.

[12] J.C. Simo, J. Oliver, and F. Armero. An analysis of strong discontinuities induced by strain-softening in rate-independent inelastic solids. *Comput. Mech.*, 12:277–296, 1993.

[13] C. Linder and F. Armero. Finite elements with embedded strong discontinuities for the modeling of failure in solids. *Internat. J. Numer. Methods Engrg.*, 72:1391–1433, 2007.

[14] F. Armero and C. Linder. New finite elements with embedded strong discontinuities for finite deformations. *Comput. Methods Appl. Mech. Engrg.*, 198:3138–3170, 2008.

[15] J. Oliver, A. Huespe, S. Blanco, and D. Linero. Stability and robustness issues in numerical modeling of material failure with the strong discontinuity approach. *Comput. Methods Appl. Mech. Engrg.*, 195:7093–7114, 2006.

[16] G.A. Francfort and J.-J. Marigo. Revisiting brittle fracture as an energy minimization problem. *Journal of the Mechanics and Physics of Solids*, 46(8):1319–1342, 1998.

[17] L. Ambrosio and V.M. Tortorelli. Approximation of functional depending on jumps by elliptic functional via γ-convergence. *Communications on Pure and Applied Mathematics*, 43(8):999–1036, 1990.

[18] A.A. Griffith. The phenomena of rupture and flow in solids. *Philos. Trans. R. Soc. Lond. Ser. A*, 221:163–198, 1921.

[19] B. Bourdin, G.A. Francfort, and J.-J. Marigo. Numerical experiments in revisited brittle fracture. *Journal of the Mechanics and Physics of Solids*, 48(4):797–826, 2000.

[20] C. Miehe, M. Hofacker, and F. Welschinger. A phase field model for rate-independent crack propagation: Robust algorithmic implementation based on operator splits. *Computer Methods in Applied Mechanics and Engineering*, 199(45-48):2765–2778, 2010.

[21] M. Ambati, T. Gerasimov, and L. De Lorenzis. A review on phase-field models of brittle fracture and a new fast hybrid formulation. *Computational Mechanics*, 55:383–405, 2015.

[22] R. Cavuoto, P. Lenarda, D. Misseroni, M. Paggi, and D. Bigoni. Failure through crack propagation in components with holes and notches: An experimental assessment of the phase field model. *International Journal of Solids and Structures*, 257:111798, 2022.

[23] L. Ambrosio. On the approximation of free discontinuity problems. *Boll. Un. Mat. Ital., B*, (7):105–123, 1992.

[24] S. Burke, C. Ortner, and E. Süli. An adaptive finite element approximation of a generalized ambrosio–tortorelli functional. *Mathematical Models and Methods in Applied Sciences*, 23(09):1663–1697, 2013.

[25] E. Tanné, T. Li, B. Bourdin, J.-J. Marigo, and C. Maurini. Crack nucleation in variational phase-field models of brittle fracture. *Journal of the Mechanics and Physics of Solids*, 110:80–99, 2018.

[26] Tota Rakesh Kumar and Marco Paggi. A robust identification procedure for phase field fracture mechanics parameters. *Theoretical and Applied Fracture Mechanics*, page 104005, 2023.

[27] V. Carollo, D. Piga, C. Borri, and M. Paggi. Identification of elasto-plastic and nonlinear fracture mechanics parameters of silver-plated copper busbars for photovoltaics. *Engineering Fracture Mechanics*, 205:439–454, 2019.

[28] C. Miehe and M. Lambrecht. Algorithms for computation of stresses and elasticity moduli in terms of seth–hill's family of generalized strain tensors. *Communications in numerical methods in engineering*, 17(5):337–353, 2001.

[29] B. Bourdin, G.A. Francfort, and J.-J. Marigo. The variational approach to fracture. *Journal of Elasticity*, 91:5–148, 2008.

[30] J. Kennedy and R. Eberhart. Particle swarm optimization. In *Proceedings of ICNN'95-international conference on neural networks*, volume 4, pages 1942–1948. IEEE, 1995.

[31] M. Clerc. The swarm and the queen: towards a deterministic and adaptive particle swarm optimization. In *Proceedings of the 1999 congress on evolutionary computation-CEC99 (Cat. No. 99TH8406)*, volume 3, pages 1951–1957. IEEE, 1999.

[32] R.C. Eberhart and Y. Shi. Comparing inertia weights and constriction factors in particle swarm optimization. In *Proceedings of the 2000 congress on evolutionary computation. CEC00 (Cat. No. 00TH8512)*, volume 1, pages 84–88. IEEE, 2000.

[33] A.R. Torrado, C.M. Shemelya, J.D. English, Y. Lin, R.B. Wicker, and D.A. Roberson. Characterizing the effect of additives to abs on the mechanical property anisotropy of specimens fabricated by material extrusion 3d printing. *Additive Manufacturing*, 6:16–29, 2015.

[34] J.-Y. Wu. A unified phase-field theory for the mechanics of damage and quasi-brittle failure. *Journal of the Mechanics and Physics of Solids*, 103:72–99, 2017.

[35] K. Pham, H. Amor, J.-J. Marigo, and C. Maurini. Gradient damage models and their use to approximate brittle fracture. *International Journal of Damage Mechanics*, 20(4):618–652, 2011.

[36] T.K. Mandal, V.P. Nguyen, and J.-Y. Wu. Length scale and mesh bias sensitivity of phase-field models for brittle and cohesive fracture. *Engineering Fracture Mechanics*, 217:106532, 2019.